AIAA-91-1760

HYPERSONIC SHOCK-WAVE TURBULENT-BOUNDARY-LAYER INTERACTION FLOWS—EXPERIMENT AND COMPUTATION

C. C. Horstman
NASA Amès Research Center
Moffett Field, CA

AIAA 22nd Fluid Dynamics, Plasma Dynamics & Lasers Conference
June 24-26, 1991 / Honolulu, Hawaii

HYPERSONIC SHOCK-WAVE TURBULENT-BOUNDARY-LAYER INTERACTION FLOWS—EXPERIMENT AND COMPUTATION

C. C. Horstman
Ames Research Center
Moffett Field, California

Abstract

Solutions of the Reynolds-averaged Navier-Stokes equations are presented and compared with experimental surface data for a series of hypersonic shock-wave/turbulent-boundary-layer interaction flows. The turbulence models used include the standard $k - \epsilon$ two-equation eddy viscosity model, a two-layer modification to this model and a third model with several modifications to account for compressibility effects. Both modified models gave significant improvements for all the test flows.

Nomenclature

a	sound speed
C_f	skin-friction coefficient
h	enthalpy
k	turbulent kinetic energy
M	Mach number
n	polytropic coefficient
p,P	pressure
q,Q	wall heat-transfer rate
S	distance along model surface
t	time
T	temperature
u,v	velocity in the x and y directions
x,y	coordinates parallel and normal to the model surface
X	distance in freestream direction
y^+	nondimensional distance from model surface, $y(\lvert\tau_w\rvert\rho_w)^{1/2}/\mu_w$
δ	boundary-layer thickness
ϵ	turbulence-energy dissipation rate
μ	laminar viscosity
μ_t	turbulent viscosity
ρ	density
τ	shear stress

Subscripts

e	boundary-layer edge
inf	free stream experimental value
o	stagnation
w	wall
∞	free stream conditions ahead of interaction
,i	partial differentiation in the ith direction

Superscripts

$(\,)'$	fluctuating quantity
$(\,)''$	mass-averaged fluctuating quantity
$\bar{(\,)}$	time-averaged quantity

Introduction

The renewed interest in hypersonic flows has made the ability to compute heating rates and the onset and extent of separation for complex flow fields imperative. Shock-wave/turbulent-boundary-layer interactions occur on many vehicle configurations of practical importance such as air-breathing inlets, wing-body junctures and deflected control surfaces. These flow fields may be separated. The successful prediction of these flow fields will be necessary in the design process to assess vehicle performance and heat protection systems.

Current turbulence modeling for high-speed flows is based on incompressible concepts and invoking Mrokovin's hypothesis. The application of these models to complex hypersonic flows is questionable. For 2-D and axisymmetric flow fields very little success has been achieved to date. No reliable data are currently available to assess 3-D hypersonic computations and their turbulence models [1].

To properly assesses and improve turbulence modeling for hypersonic speeds, detailed experimental data are required which include both mean and fluctuating flow-field measurements. However limited data are available for hypersonic speeds and most of these data are for 2-D or axisymmetric flows. We at NASA Ames are currently expanding this data base for both 2- and 3-D flow fields. Following a thorough literature search and evaluation process [1], five experimental investigations have been identified that can be used to test the accuracy of the various prediction methods at Mach numbers above 6. Four of these investigations were 2-D or axisymmetric. The measurements include surface pressure, skin-friction and heat transfer, but only limited mean flow-field data and no turbulence measurements. To these four investigations the data from a recent experimental study conducted at NASA Ames have been added.

This paper uses a 2-D/axisymmetric Navier-Stokes code to study the accuracy of the two-equation $k-\epsilon$ turbulence model when compared to the experimental data. Also two modifications of the standard $k-\epsilon$ model are investigated. The first is the new two-layer $k-\epsilon$ model developed by Rodi [2] which has had good success for separated flows at low speeds. The second is a modification developed to account for compressibility effects following the work of Rubesin [3] and Vuong and Coakley [4]. These three models are evaluated by comparison with the data. The relative merits of the modifications are discussed.

This investigation is a first step toward the improvement of turbulence models for hypersonic shock-wave/turbulent-boundary-layer interaction flows. Hopefully the experimental data base with its wide range of geometries, Mach numbers, wall-to-stagnation temperature ratios and Reynolds numbers will be sufficient to properly assess the proposed turbulence models and provide insight for future improvements.

Turbulence Models

The eddy-viscosity turbulence models used for the present computations include the Jones-Launder $k-\epsilon$ model [5] and two modifications of this model. These models are described below.

The two-equation $k-\epsilon$ turbulence model is expressed as

$$\frac{D\rho k}{Dt} = \mu_t\left[S_{ij}S_{ij} - \frac{2}{3}\,\mathrm{div}\,\vec{u}^2\right] - \frac{2}{3}\rho k\,\mathrm{div}\,\vec{u} - \rho\epsilon + \mathrm{diffusion} + \mathrm{LRT} \tag{1}$$

$$\frac{D\rho\epsilon}{Dt} = \frac{\epsilon}{k}\left[C_1\mu_t\left(S_{ij}S_{ij} - \frac{2}{3}\,\mathrm{div}\,\vec{u}^2\right) - C_1\frac{2}{3}\rho k\,\mathrm{div}\,\vec{u}\right] - C_2 f_2 \rho\frac{\epsilon^2}{k} + \mathrm{diffusion} + \mathrm{LRT} \tag{2}$$

$$S_{ij} = u_{i,j} + u_{j,i} \tag{3}$$

$$\mu_t = C_\mu \rho k^2/\epsilon \tag{4}$$

where LRT refers to the low Reynolds number terms used near solid surfaces. The values used for the constants were $C_1 = 1.44$, $C_2 = 1.92$, and $C_\mu = 0.09$.

The second model used here is the two-layer model developed by Rodi and his co-workers [2]. For this model the ϵ equation is replaced by an analytical expression near the wall. In the wall region this model determines the eddy viscosity from the relation

$$\mu_t = f_\mu C_\mu \rho \sqrt{k}\, L \tag{5}$$

$$f_\mu = 1 - \exp(-0.0198\, R_y) \tag{6}$$

$$R_y = \rho \sqrt{k}\, y / \mu \tag{7}$$

where y is the normal distance to the wall. The dissipation rate ϵ is given by

$$\epsilon = \frac{k^{3/2}}{L}\left(1 + \frac{13.2}{\rho \sqrt{k}\, L/\mu}\right) \tag{8}$$

The length scale L is assumed proportional to the distance from the wall, i.e., $L = C_r y$. The wall region model is matched with the full $k - \epsilon$ model at a distance from the wall where $R_y = 150$ ($f_\mu \approx 0.95$). At this location the eddy viscosity given by Eqn. 4 is equated to Eqn. 5 to determine the proportionality constant C_r. For typical shock-wave/boundary-layer interaction flows solved here C_r varied from 0.8 to 9.0 at various locations in the flow field. The lowest values occurred upstream of the interaction and the highest near reattachment. For the present computations, maximum and minimum limits of 2.4 and 1.2 were used for C_r. With these limits imposed, the values of eddy viscosity are no longer matched between the inner and outer models for large regions of the flow field. A few solutions were obtained using $C_r = 2.4$ which is equivalent to using the Prandtl length scale. (Rodi [2] used a constant value of 2.45 in his incompressible computations). Solutions were also obtained for several interaction flows varying the match point from $R_y = 100$ to 200. These results differed from each other by less than 3 percent.

The third model is composed of two compressibility corrections, one suggested by Rubesin [3] and the other by Monsour and Kline [6], which was first implemented by Vuong and Coakley [4]. Rubesin's corrections model the additional terms which appear in the turbulent kinetic energy equation after mass averaging. These additional terms, in the right-hand side of the equation, are

$$\text{NEW TERMS} = -\overline{u_i''}\,\overline{p}_{,i} + \overline{p' u''_{i,i}} + D_k \tag{9}$$

In Ref. 3 expressions for these terms are developed. The thin-layer version of these terms (used for the present computations) is shown below

$$\overline{u_i''}\,\overline{p}_{,i} = C_{K_1} \frac{\gamma - 1}{n - 1} \frac{C_e}{\bar{a}^2} \frac{d\bar{p}}{dx} \frac{\bar{k}^3}{\bar{\epsilon}^2} \frac{\partial \bar{h}}{\partial y} C_\mu \frac{\partial \bar{u}}{\partial y} \tag{10}$$

$$\begin{aligned} \overline{p' u''_{i,i}} = C_{K_2}\, n \frac{\gamma - 1}{n - 1} \frac{C_e}{\bar{a}^2} \frac{\bar{p}}{\bar{\rho}} \frac{\bar{k}^2}{\bar{\epsilon}} \frac{\partial \bar{h}}{\partial y} \\ \times \left(\frac{\partial \bar{\rho}}{\partial y} - C_\mu \frac{\bar{k}}{\bar{\epsilon}} \frac{\partial \bar{\rho}}{\partial x} \frac{\partial \bar{u}}{\partial y} \right) \\ - C_{K_3} C_e^2 \frac{n}{2(n-1)^2} \bar{\rho}\, \bar{v} \\ \times \left[\frac{1}{\bar{h}^2} \frac{\bar{k}^3}{\bar{\epsilon}^2} \left(\frac{\partial \bar{h}}{\partial y} \right)^2 \right], y \end{aligned} \tag{11}$$

$$D_K = C_{K_4} \left\{ \left[C_s \bar{\rho} \frac{\bar{k}^2}{\bar{\epsilon}} + \mu \right] \frac{\partial \bar{k}}{\partial y} \right\}, y \tag{12}$$

For the above equations the x, y coordinates are considered parallel and normal to the wall respectively.

The new terms (Eqns. (10), (11) and (12)) are added to the right-hand side of the turbulent kinetic energy equation, Eqn. (1). The new terms are also added to the ϵ equation multiplied by ϵ/k and replacing D_k with D_ϵ where

$$D_\epsilon = C_{K_4} \left\{ \left[C_v \bar{\rho} \frac{\bar{k}^2}{\bar{\epsilon}} + \mu \right] \frac{\partial \bar{\epsilon}}{\partial y} \right\}, y \tag{13}$$

Rubesin [7] has recommended these values for the following constants, $n = -0.4$, $C_s = 0.25$, $C_e = 0.25$. The

constants $C_{K_{1-4}}$ are arbitrary constants added by the author and were determined by comparing the results with experimental data. Computations were made systematically varying $C_{K_{1-4}}$ for two specific test flows (the M = 7 cylinder flare data at flare angles of 20 and 32.5 degrees). The values chosen were $C_{K_1} = 4.0$, $C_{K_2} = -1.0$, $C_{K_3} = 0.0$, and $C_{K_4} = 0.25$. These values, which gave good agreement with the two specific test flows, were used for all subsequent computations. Note that the values used are by no means unique and it is probable that another set could give better overall results. Finite values of C_{K_3} produced spatial oscillations in the solution downstream of the shock wave and therefore C_{K_3} was set equal to zero. Physically this neglects the variance of density fluctuations as compared to the mean density gradients in the rate of strain term (Eqn. (11)).

In addition to the compressibility corrections suggested by Rubesin (discussed above) the third model also incorporates a correction to the turbulent length scale, following the work of Vuong and Coakley [4]. In this modification, an upper bound is placed on the length scale appearing in the eddy viscosity such that it can never be greater than a constant times the Prandtl length scale in the wall region. This is derived by bounding the viscosity given by the $k - \epsilon$ model by the turbulent viscosity as determined by Prandtl's model, and by assuming the Bradshaw relation between shear stress and kinetic energy and the logarithmic law for velocity to hold; that is,

$$\mu_t = C_\mu \rho \frac{k^2}{\epsilon} = C_\mu \rho \sqrt{k}\, \ell < \rho(\kappa y)^2 \left|u_y\right| \qquad (14)$$

$$\tau / \rho k = C_\mu^{1/2} = u_\tau^2 / k, \qquad \left|u_y\right| = u_\tau / \kappa y \qquad (15)$$

The result of this limitation is the following relation (for $\kappa = 0.4$ and $C_\mu = 0.09$), which was used in place of ℓ appearing in the above formula for eddy viscosity

$$\ell = \min\left(2.4y, \frac{k^{3/2}}{\epsilon}\right) \qquad (16)$$

For the present calculations this limit was also used to limit the turbulent kinetic energy using ℓ defined by Eqn. (16) above and redefining kinetic energy by the following relation.

$$k = (\epsilon \ell)^{2/3} \qquad (17)$$

The above length scale modifications generally do not change the predictions except near a reattachment point and to a lesser extent near a separation point. For equilibrium attached flows the length scale predicted by the $k - \epsilon$ model is approximately equal to 2.4y in the wall region.

The corrections described above comprise the third modification for the remainder of this paper. This model will be called the "compressible" model. The terms developed by Rubesin (Eqns. (9 - 13)) which are added to the right-hand side of the k and ϵ equations have the principal effect of increasing the separation zone for all the test cases computed. The length scale limitation also slightly increases the separation zone but its principal function is to limit the large overshoots in heat transfer near reattachment. Examples will be shown later.

Description of Computations

The partial differential equations used to describe the mean flow field are the time-dependent, mass-weighted, Reynolds-averaged, Navier-Stokes equations for 2-D or axisymmetric flow. The above discussed turbulence models were used for closure. The numerical procedure chosen here is the MacCormack explicit-implicit, second-order predictor-corrector, finite-volume method [8].

Each computational domain consisted of a uniform mesh spacing in the streamwise direction. In the vertical direction, a geometrically stretched spacing was used near the wall, followed by a uniform spacing. The total mesh size varied from 80 to 150 points in the x direction and from 36 to 60 points in the y direction, depending on the test flows solved. The mesh spacing in the x direction varied from 0.1 to 0.3 times the incoming boundary layer thickness. Approximately 30 points in the y direction were used to resolve the upstream boundary layer, resulting in as few as 20 points to resolve the boundary layer downstream of the interaction. The values of y^+ for the first mesh point varied from 0.005 to 0.2. A few cases were computed with both a 40×100 and a 60×150 mesh. No change was observed in the results providing Δx was less than 0.3δ, the first y mesh point was less than $y^+ = 0.15$, and at least 20 points were always located in the boundary layer. A separate grid study was also done to determine the largest value of y^+ for the first point that could be used for each turbulence model. A sample of the results are shown in Fig. 1. Here, the calculated peak value of heat transfer normalized by the calculated value for $y^+ = 0.15$ is plotted versus y^+ for a M = 7 test flow using the three turbulence models. For

the standard $k - \epsilon$ model small increases in y^+ can produce very large errors in heat transfer. However, for the two-layer and compressible models only a small increase in heat transfer is evident for y^+ up to 0.5. This is because both these models use analytic length scales near the wall. Computed skin-friction results show the same thing.

The upstream boundary conditions were prescribed by uniform freestream conditions (or the oblique shock conditions) plus a boundary-layer profile matching the experimental boundary-layer displacement thickness at a location well upstream of the interaction region. At the downstream boundary, the gradients of the flow variables in the streamwise direction were set equal to zero. At the wall, no-slip and constant wall temperature were applied. The turbulent kinetic energy and dissipation were set equal to zero at the wall. At the upper boundary, conditions were held fixed. Typical computing times for the fully vectorized code on the Cray YMP/single processor were 25 minutes.

New Experimental Results

The experiment was conducted in the NASA Ames 3.5-Foot Hypersonic Wind tunnel. The nominal free stream test conditions were: total temperature = 1166 K, total pressure = 60 atm, free stream Reynolds number = 5.0×10^6/m, and local free stream Mach number = 8.2. The test core diameter was approximately 0.6 m. The test model consisted of a sharp flat plate and a shock generator (see Fig. 2). The flat plate was 76 cm wide, 220 cm long, and 10 cm thick with a 10 degree wedge at the leading edge. The entire plate was water-cooled, maintaining a constant surface temperature of 300 K during a run. Instrumentation, consisting of pressure taps and two types of heat transfer gages, was located along the plate centerline. Boundary-layer survey ports were also located in the plate. Several shockwave generator angles were tested varying from 5 to 11 degrees. The leading edge of the generator was located between 120 and 140 cm from the leading edge depending on the shock angle.

Flow quality, extent of two dimensional flow, and verification of an incoming equilibrium turbulent boundary layer were verified by detailed flow field surveys and surface oil flow, pressure, and heat transfer measurements. For the shock interaction cases the data only include surface pressure and heat transfer. Further details of this experimental investigation along with new 3-D data are in Ref. 9.

Results and Discussion

Seven 2-D and axisymmetric experimental investigations were chosen for the current turbulence model evaluation process (see Fig. 3). These investigations include all four hypersonic studies recommended by Settles and Dobson [1] plus a recommended supersonic compression corner case, an axisymmetric flare study, and the new impinging shock study described above. The first experiment, conducted by Settles et al [10], is a compression corner tested at Mach 3. The second, conducted at M = 6.8 by Kussoy and Horstman [11], is the interaction of an incident axisymmetric shock-wave on a cylinder. The third was conducted at M = 7 by Kussoy and Horstman [12] on an axisymmetric cone cylinder flare. Next are the new experimental data for an impinging shock at Mach 8. Two experiments were conducted at M = 9.2 by Coleman [13,14] on an axisymmetric hollow cylinder flare and a 2-D compression corner. Finally, the M = 11 and 13 cone flare data obtained by Holden et al [15] will also be used to evaluate the computations. For all the flows above either the flare, corner, or incident shock angles were varied to obtain flow fields with and without separation. Solutions were obtained using the three turbulence models described previously for 21 test cases. Only representative results will be shown here.

Comparisons of the upstream zero-pressure-gradient predictions of skin friction and heat transfer with the measured results are shown in Fig. 4. Plotted are the calculated values of skin friction and heat transfer normalized by the experimental values as a function local boundary layer edge Mach number for each experimental investigation. Results for three turbulence models are shown. Averaging these results the standard $k - \epsilon$ model underpredicts skin friction by 9% and heat transfer by 11%. The compressible model underpredicts by 17% and 20% respectively and the two-layer model with variable C_r underpredicts by 34% and 36% respectively. However when the two-layer model fixes the constant $C_r = 2.4$, its prediction shows a substantial improvement (solid symbols in Fig. 4). It must be noted that no error limits exist for the heat transfer data at Mach numbers greater than 8. Therefore it is difficult to assess the accuracy of the computations at the highest Mach numbers.

Comparisons of the computations and experiment for eight selected test cases are shown in Figs. 5-12. In all cases the data and computations are normalized by the same number for each test flow, namely, the average experimental value ahead of the interaction. For each test case, solutions for the three turbulence models are shown. The legend shown in Fig. 5 is the same for all the figures.

The test cases in Figs. 7 and 8 were used to fix the constants ($C_{K_{1-4}}$) in the compressible model and set the limits for C_r in the two-layer model. Also shown are the predicted and measured separation zone sizes for three studies as a function of shock wave strength (Figs. 13-14). Rather than discuss the individual test cases we will make several general observations which are valid for most or all the comparisons (including the 13 additional test cases not shown here).

The results obtained using the standard $k - \epsilon$ model underpredict the separation size and overpredict the skin friction and heat transfer near reattachment for the separated cases by substantial amounts and also in the adverse pressure gradient regions for attached cases. The compressible model is at all times an improvement or at least equal to the standard $k - \epsilon$ model. The compressible modifications increase separation size and decrease skin friction and heat transfer at reattachment and in adverse pressure gradient regions to give better agreement with experiment. The original intent of the two-layer model was to save computer time by allowing a more coarse mesh to be used [2]. For the present hypersonic computations this did not prove to be the case. The mesh requirements for this model are almost identical to the standard model. However the computed results using this model did increase the predicted separation size and lower the skin friction and heat transfer at reattachment, similar to the compressible model. But in regions of zero and low pressure gradient the computed results tend to be too low (Figs. 4 and 12). Other than this defect the results also are better or equal to the results using the standard model.

To examine the effects of the individual modifications in the compressible model, a few solutions were with the Rubesin corrections alone (Eqns. 10-13) and with the length scale corrections alone (Eqns. 16-17). These solutions are shown in Fig. 16 for the M = 7, 35 degree flare case (same as Fig. 8). Also shown are the standard and compressible model results. It is seen that both the Rubesin and length scale modifications increase separation size and are essentially additive for the combined solution. Only the length scale correction changes the heat transfer in the reattachment region.

Figure 17 shows the effect of using $C_r = 2.4$ in the two-layer model for the same test flow discussed above. Also shown are the standard and variable C_r solutions. The only significant change for the constant C_r solution is the collapse of the separation region back to the standard solution. These results suggest the formulation of a new two-layer model where C_r is held constant equal to 2.4 in low pressure gradient zones and allowed to vary in strong adverse pressure gradient regions. This was not attempted in the present study.

Conclusions

Solutions of the Reynolds-averaged Navier-Stokes equations using three turbulence models, including a model modified to account for compressibility effects, have been compared with several hypersonic shock-wave/turbulent-boundary-layer interaction test flows. The data available for comparison included surface pressure and heat transfer and the length of the separation zones. No single model accurately predicted all the test cases. However both the modified compressible model and the two-layer model showed substantial improvement over the standard $k - \epsilon$ model and could certainly be used to predict unknown shock-wave/boundary-layer interaction flows with reasonable confidence. Considering the experimental errors present in the data (several experiments do not even try to estimate their errors) and the ever-present computational errors due to numerical approximations and smoothing, the new compressible turbulence model described here is certainly more than adequate to solve these types of flowfields. Further improvements in turbulence modeling await a more complete data base which includes detailed fluctuating flow velocity, density and temperature measurements. Experiments are currently in progress at NASA Ames and elsewhere to provide these data.

References

1. Settles, G. S. and Dodson, L. J., "Hypersonic Shock/Boundary Layer Interaction Database," AIAA Paper 91-1763, Honolulu, HI, June 1991.

2. Rodi, W., "Experience with Two-Layer Models Combing the $k - \epsilon$ Model with a One-Equation Model Near the Wall," AIAA Paper 91-0216, Reno, NV, Jan. 1991.

3. Rubesin, M. W., "Extra Compressibility Terms for Favre-Averaged Two-Equation Models of Inhomogeneous Turbulent Flows," NASA Contractor Report 177556, June 1990.

4. Vuong, S. T. and Coakley, T. J., "Modeling of Turbulence for Hypersonic Flow With and Without Separation," AIAA Paper 87-0286, Reno, NV, Jan. 1987.

5. Jones, W. P. and Launder, B. E., "The Prediction of Laminarization with a Two-Equation Model of turbulence," International J. Heat and Mass Transfer, Vol. 15, Feb. 1972, pp. 301-314.

6. Kline, S. J., Cantwell, B. J. and Lilley, G. M., Proceedings of the 1980-81AFOSR-HTTM Stanford Conference on Complex Turbulent Flows, Vol. 1, Stanford University, Stanford, CA, 1981.

7. Rubesin, M. W., personal communication.

8. MacCormack, R. W., "Numerical Method for Solving the Equations of Compressible Viscous Flow," AIAA J., Vol. 20, Sept. 1982, pp. 1275-1281.

9. Kussoy, M. I. and Horstman, K. C., "Documentation of Two- and Three-Dimensional Shock Wave/ Turbulent Boundary Layer Interaction Flows at Mach 8.2," to be published as NASA TM.

10. Settles, G. S., Vas, I. E. and Bogdonoff, S. M., "Details of a Shock-Separated Turbulent Boundary Layer at a Compression Corner," AIAA J., Vol. 14, Dec. 1976, pp. 1709-1715.

11. Kussoy, M. I. and Horstman, C. C., "An Experimental Documentation of a Hypersonic Shock-Wave Turbulent Boundary Layer Interaction Flow-With and Without Separation," NASA TM-X-62,412, Feb. 1975.

12. Kussoy, M. I. and Horstman, C. C., "Documentation of Two- and Three-Dimensional Hypersonic Shock Wave/Turbulent Boundary Layer Interaction Flows," NASA TM-101075, Jan. 1989.

13. Colemen, G. T. and Stollery, J. L., "Heat Transfer in Hypersonic Turbulent Separated Flow," I.C. Aero Report 72-05, Imperial College of Science and Technology, London, March 1972.

14. Coleman, G. T., "A Study of Hypersonic Boundary Layers over a Family of Axisymmetric Bodies at Zero Incidence: Preliminary report and Data Tabulation," I.C. Aero Report 73-06, Imperial College of Science and Technology, London, Sept. 1973.

15. Holden, M. S., Havener, A. G. and Lee, C. H. "Shock Wave/Turbulent Boundary Layer Interaction in High-Reynolds-Number Hypersonic Flows," CUBRC-86681, 1986.

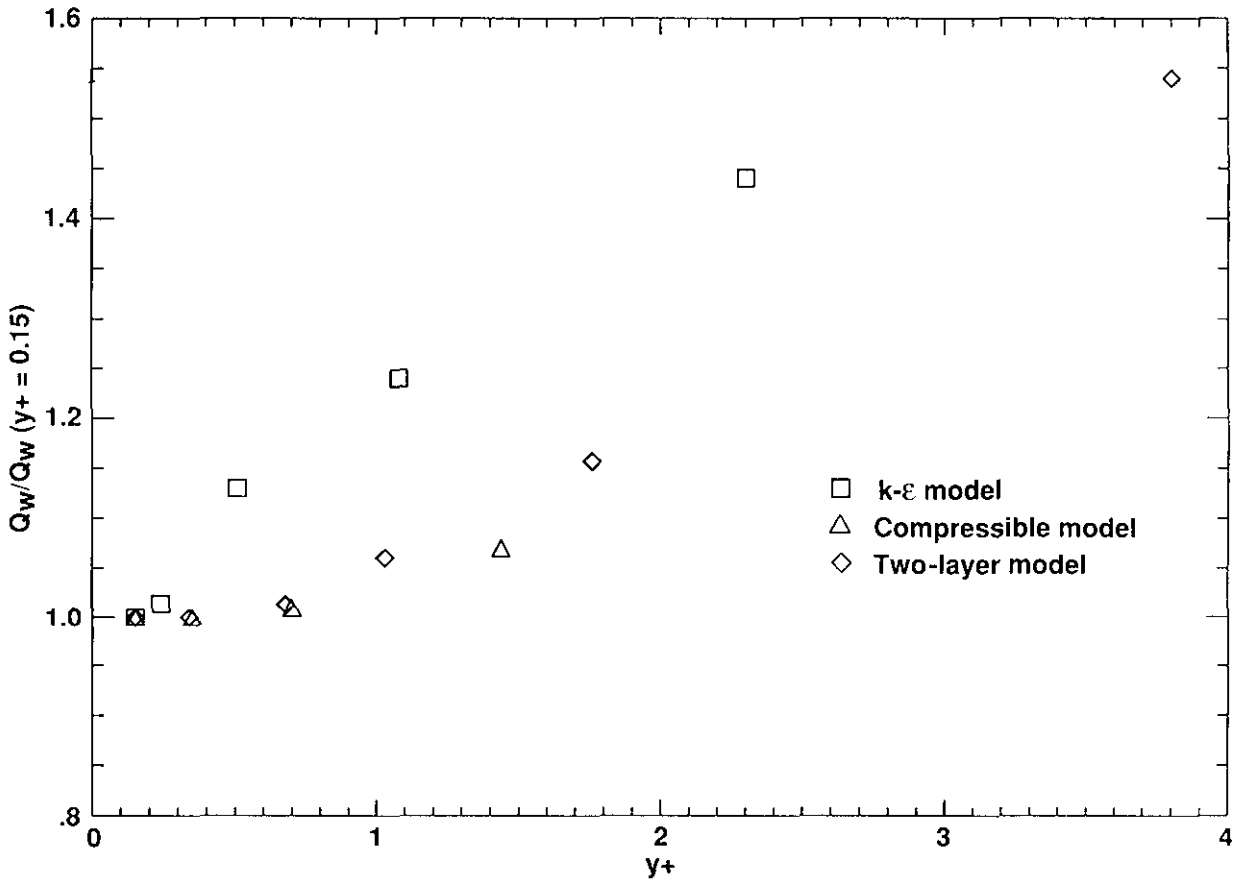

Fig. 1 Grid resolutions effects, M = 7.

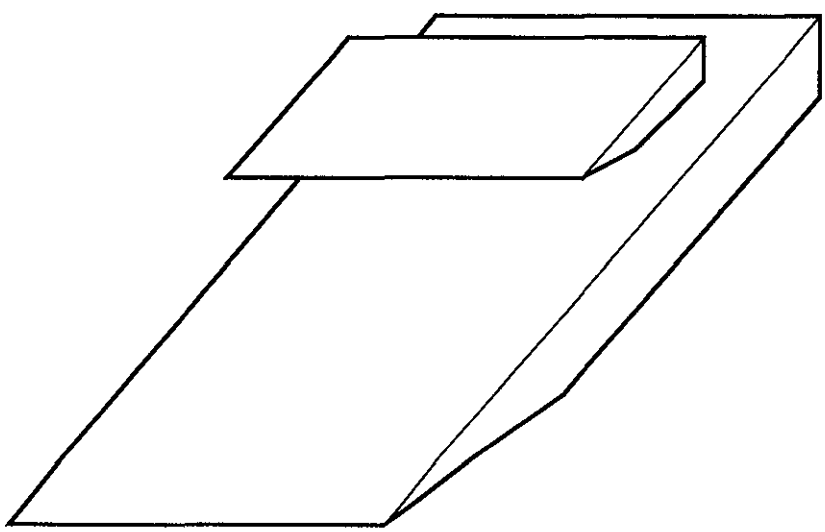

Fig. 2 Test model.

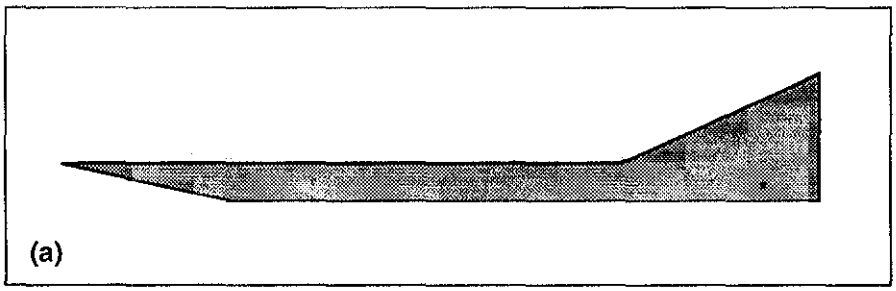

2-D Compression Corner
Settles, G.S. et. al.
$M_\infty = 2.85$, $T_W/T_O = 1.06$

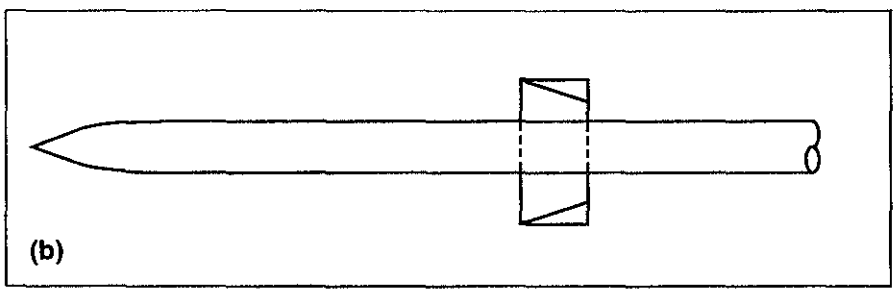

Axisymmetric Impinging Shock
Kussoy, M.I. & Horstman, C.C.
$M_e = 6.7$, $T_W/T_O = 0.43$

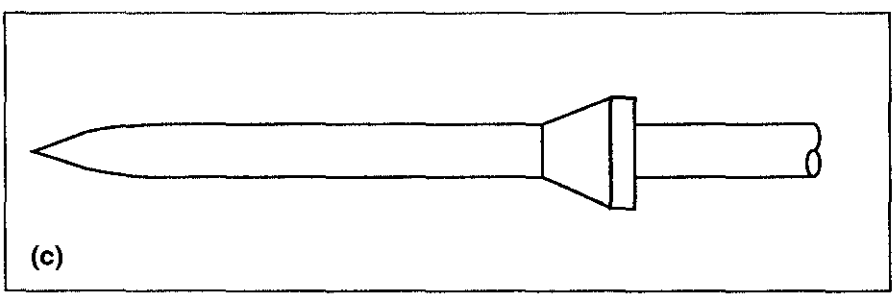

Axisymmetric Cylinder-Flare
Kussoy, M.I. & Horstman, C.C.
$M_e = 7.1$, $T_W/T_O = 0.35$

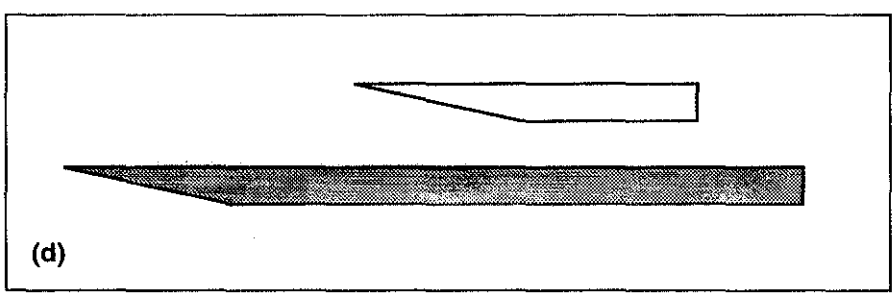

2-D Impinging Shock
Kussoy, M.I. & Horstman, K.C.
$M_e = 8.2$, $T_W/T_O = 0.27$

Fig. 3 Experimental test flows.

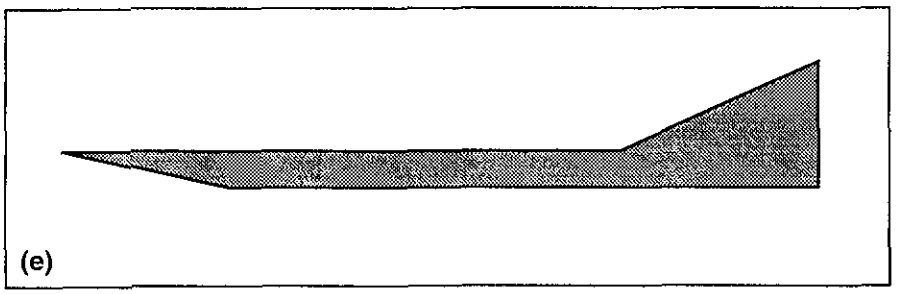

2-D Compression Corner
Coleman, G.T. & Stollery, J.L.
$M_\infty = 9.2$, $T_W/T_O = 0.25$

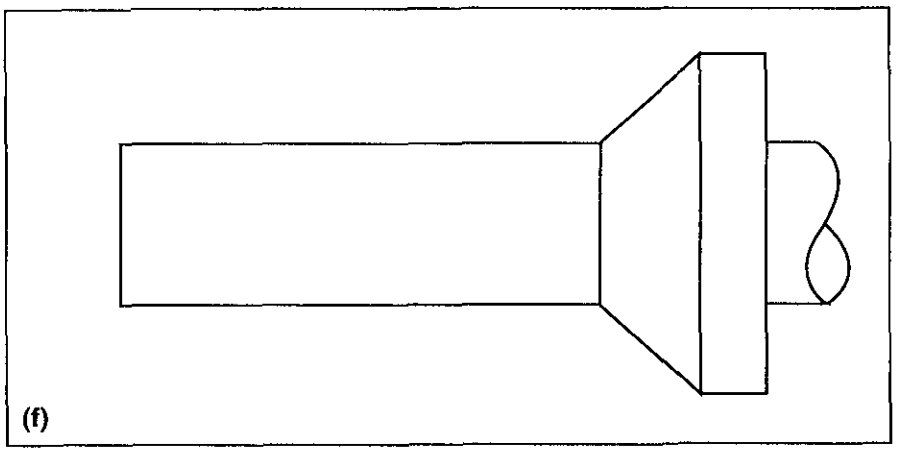

Axisymmetric Cylinder-Flare
Coleman, G.T.
$M_\infty = 9.2$, $T_W/T_O = 0.25$

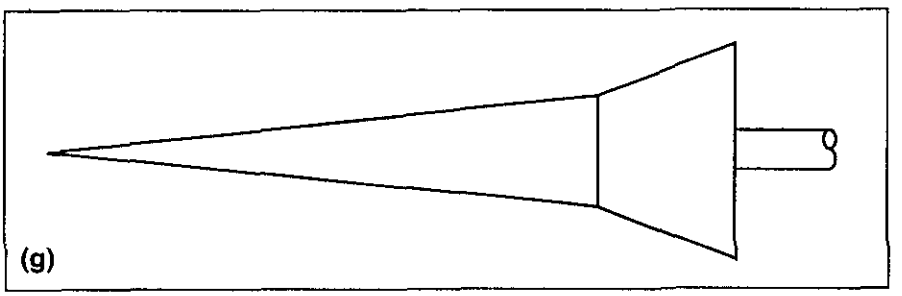

Axisymmetric Cone-Flare
Holden, M.S. et. al.
$M_e = 9.2$, $T_W/T_O = 0.20$
$M_e = 10.3$, $T_W/T_O = 0.17$

Fig. 3 Concluded.

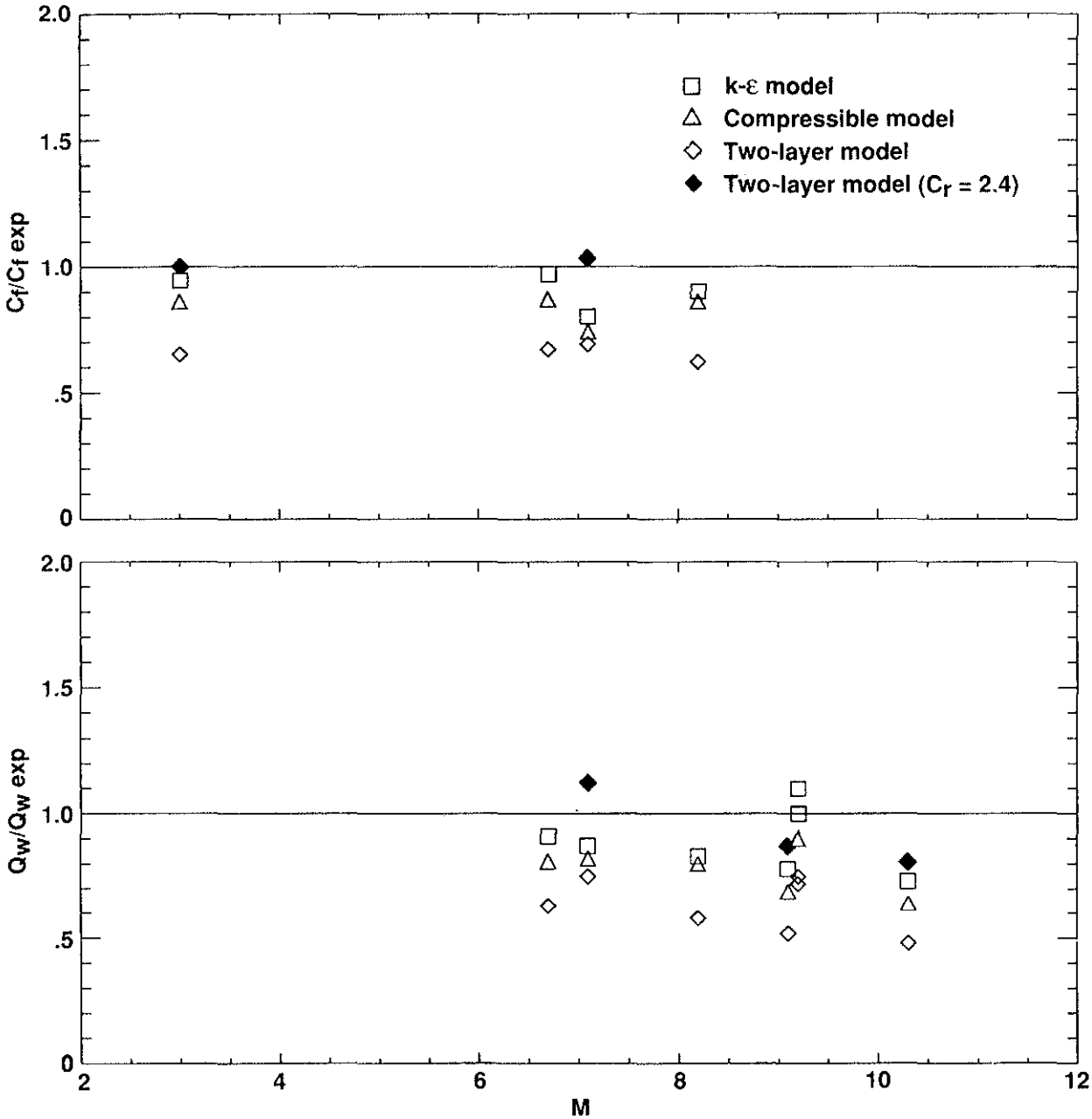

Fig. 4 Zero pressure gradient predictions.

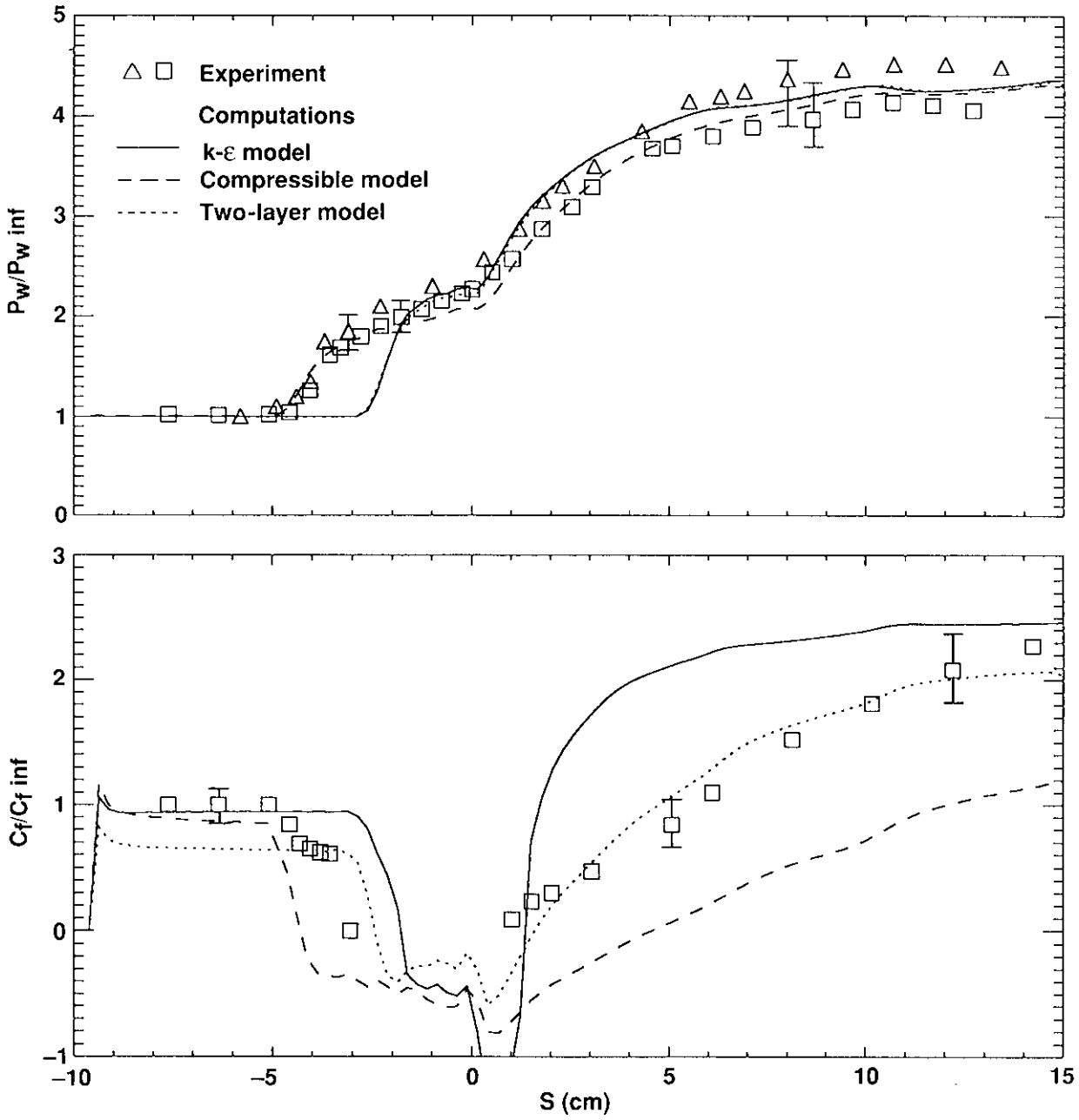

Fig. 5 Comparisons of surface pressure and skin friction distributions, M = 2.85, 24° compression corner flow.

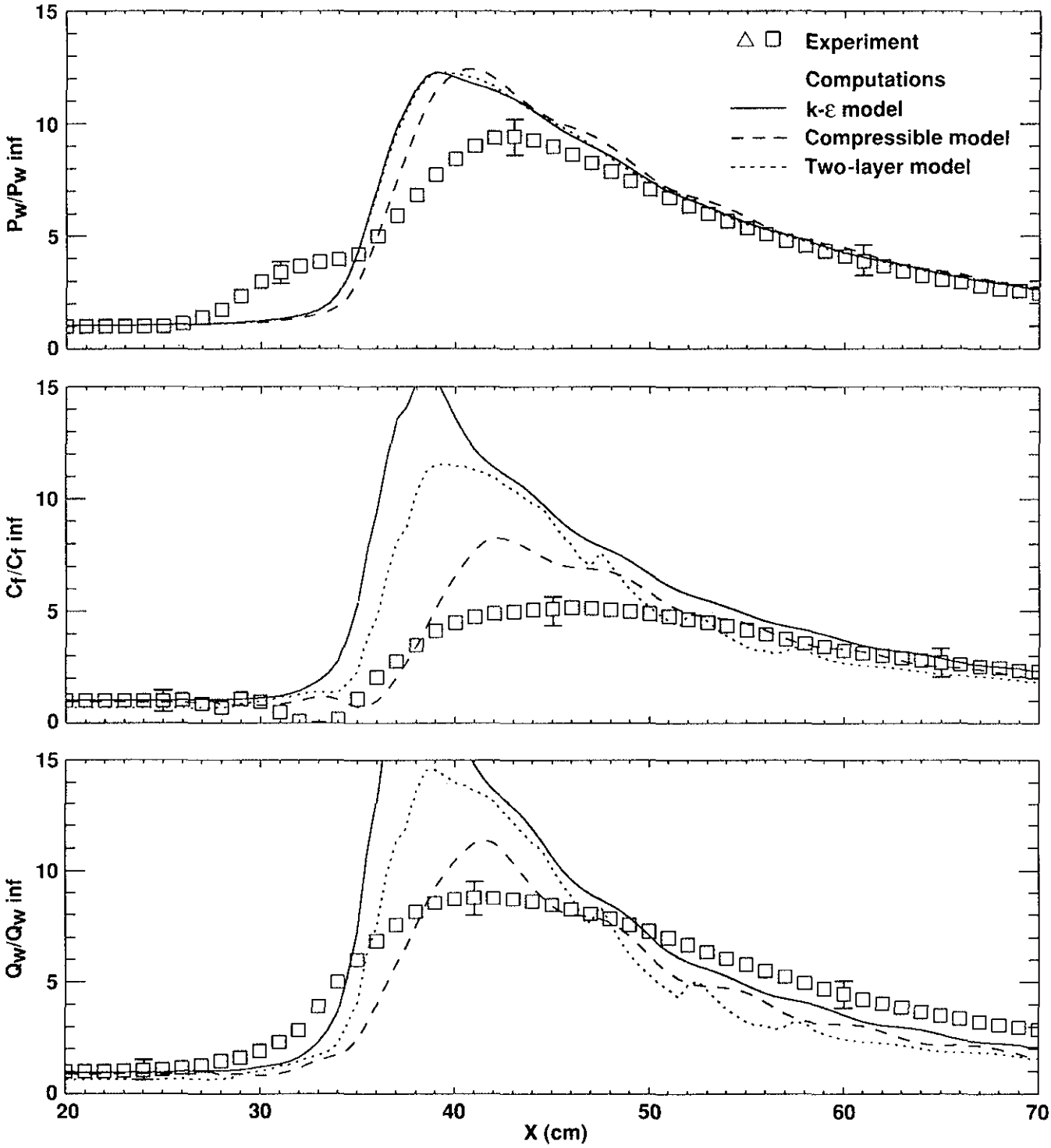

Fig. 6 Comparisons of surface pressure, skin friction and heat transfer distributions, M = 6.7, 15° axisymmetric impinging shock flow.

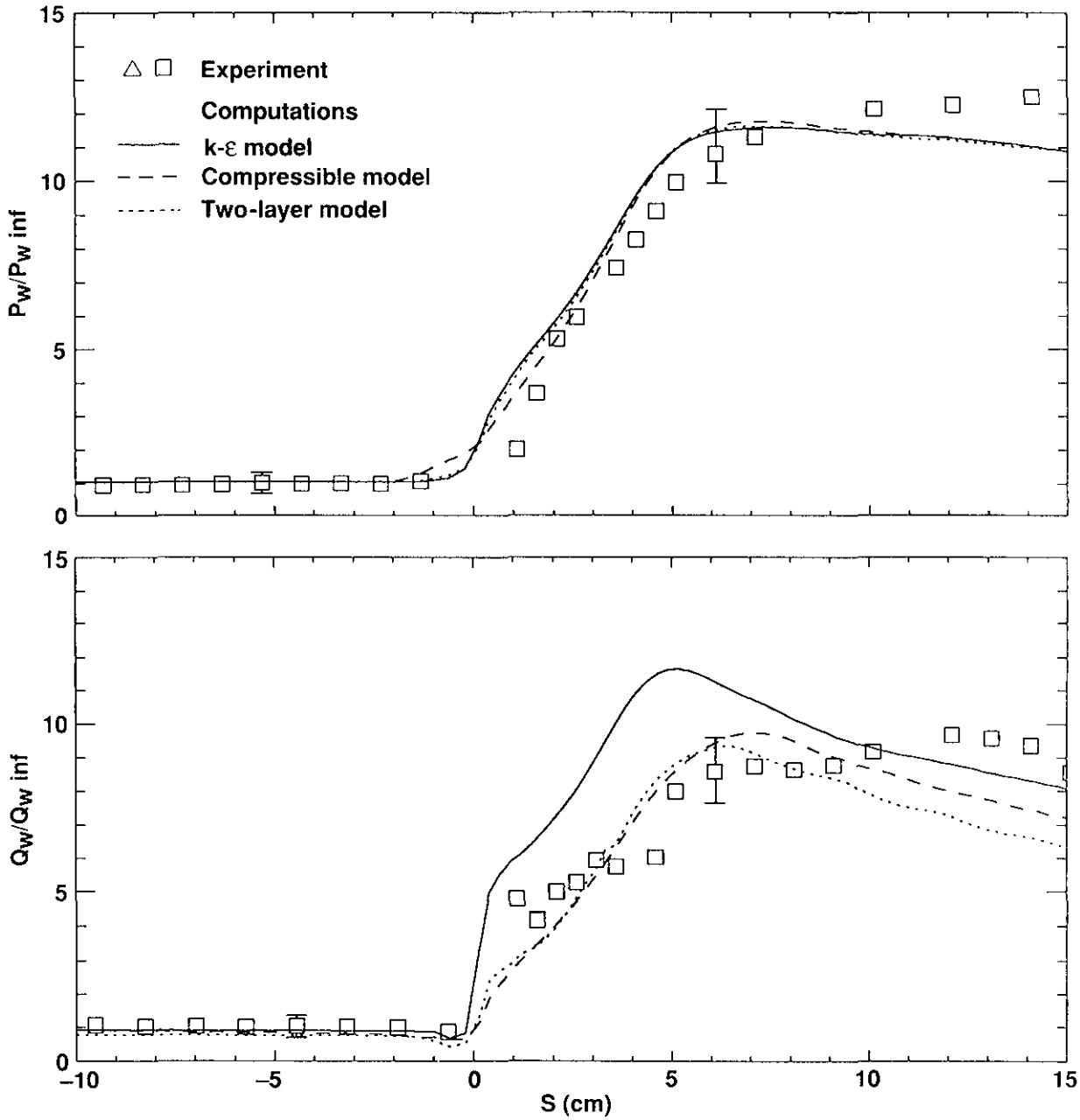

Fig. 7 Comparisons of surface pressure and heat transfer distributions, M = 7.1, 20° cylinder-flare flow.

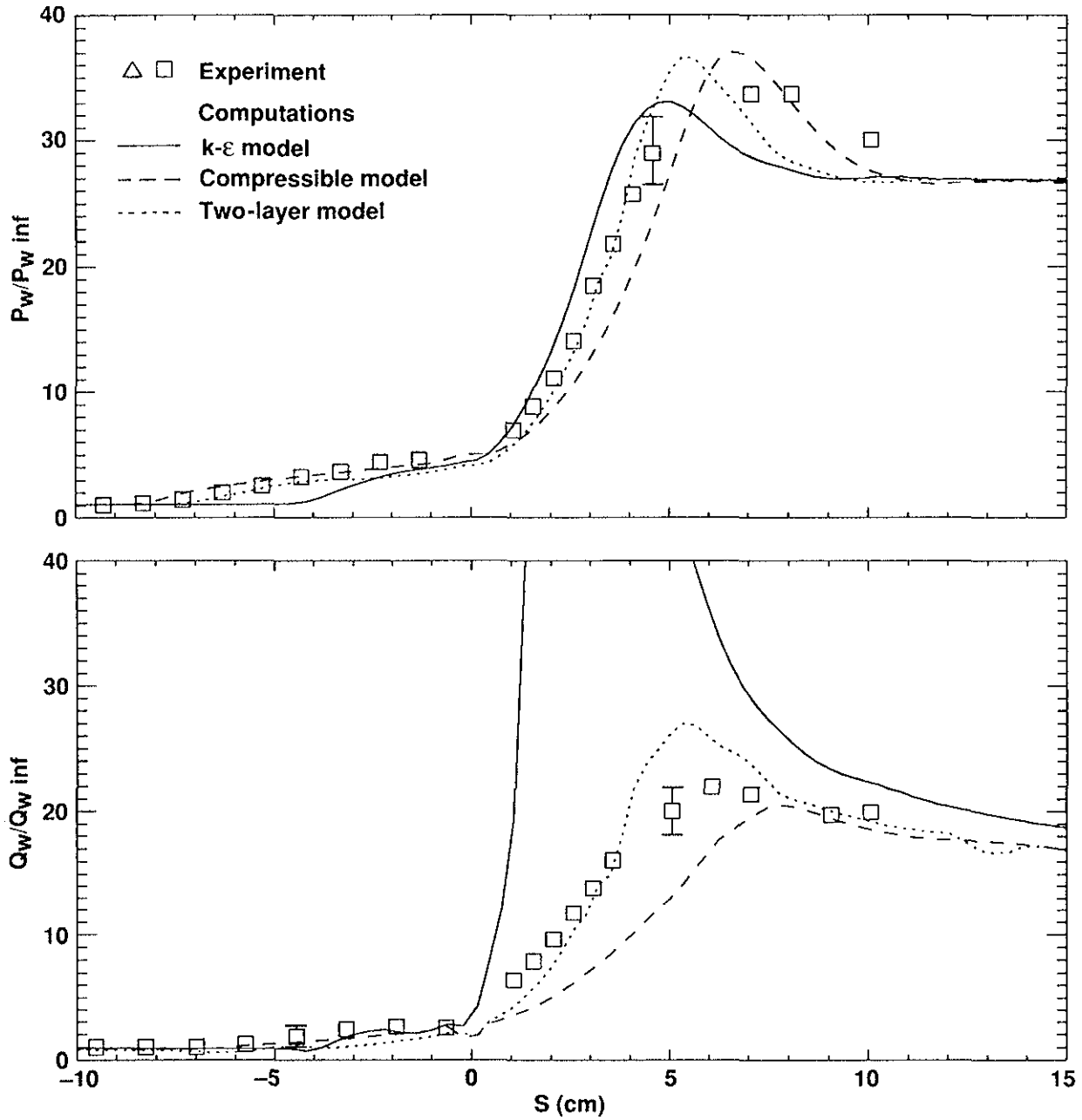

Fig. 8 Comparisons of surface pressure and heat transfer distributions, M = 7.1, 35° cylinder-flare flow.

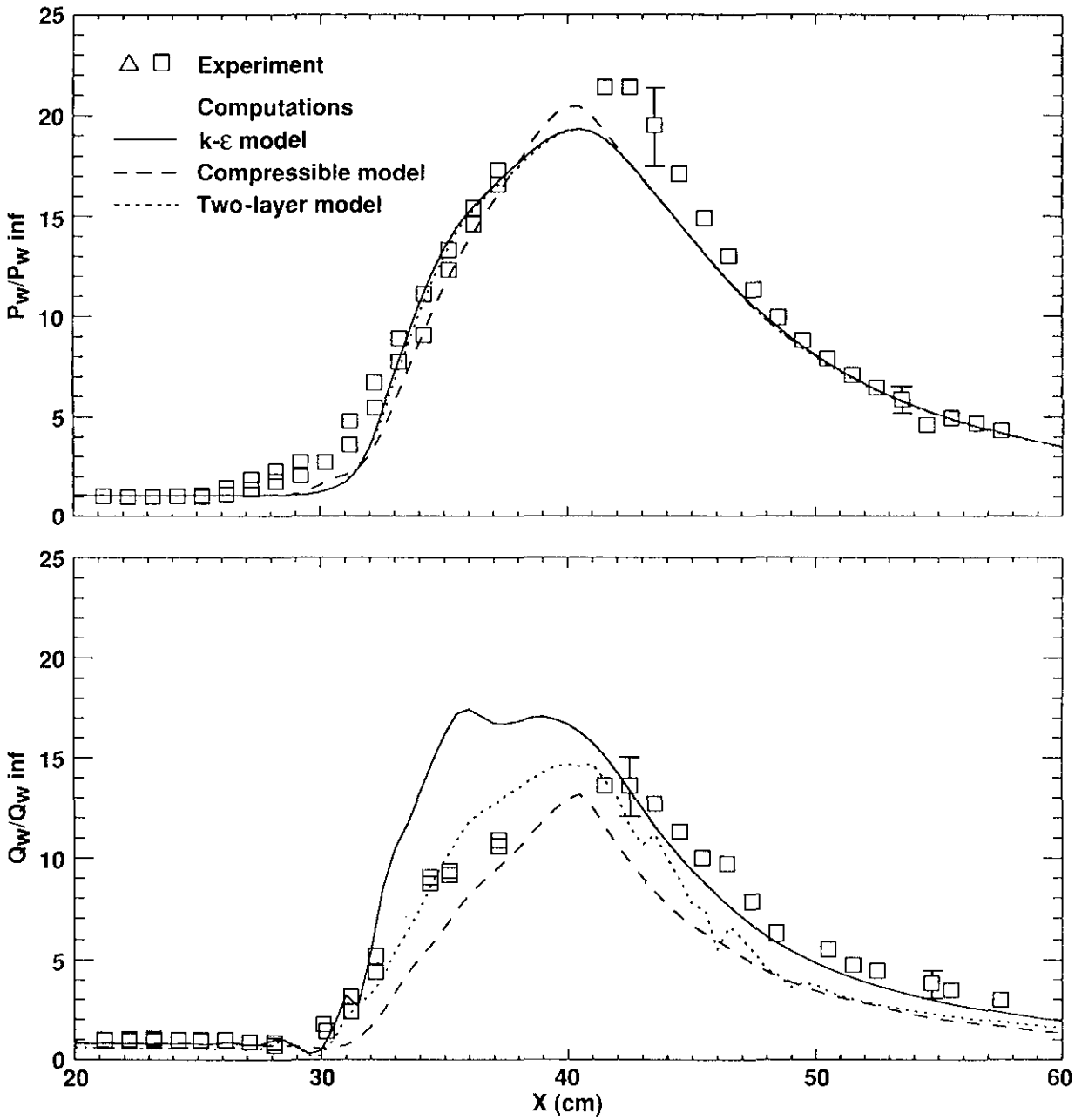

Fig. 9 Comparisons of surface pressure and heat transfer distributions, M = 8.2, 10° imping shock flow.

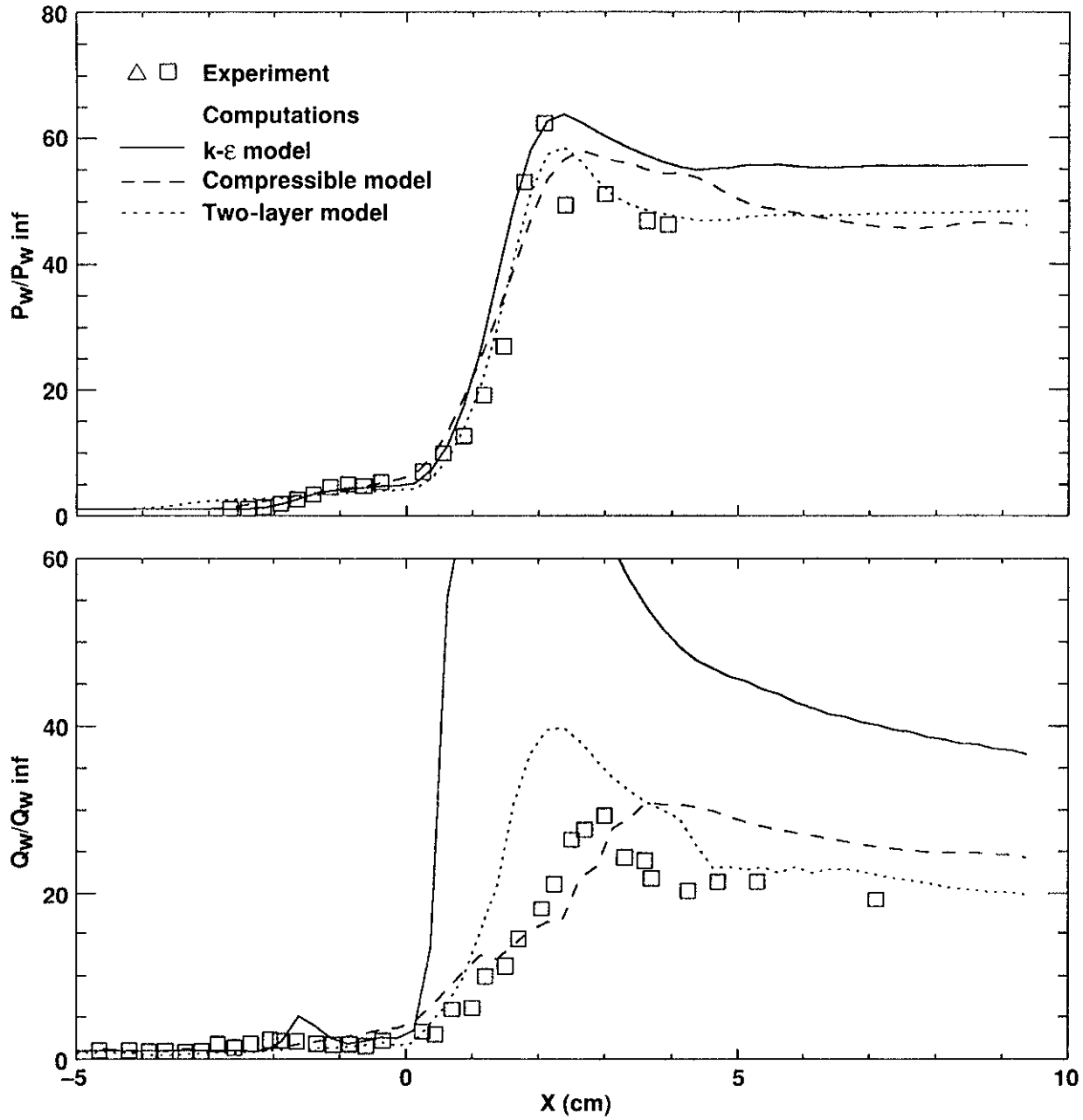

Fig. 10 Comparisons of surface pressure and heat transfer distributions, M = 9.2, 34° compression corner flow.

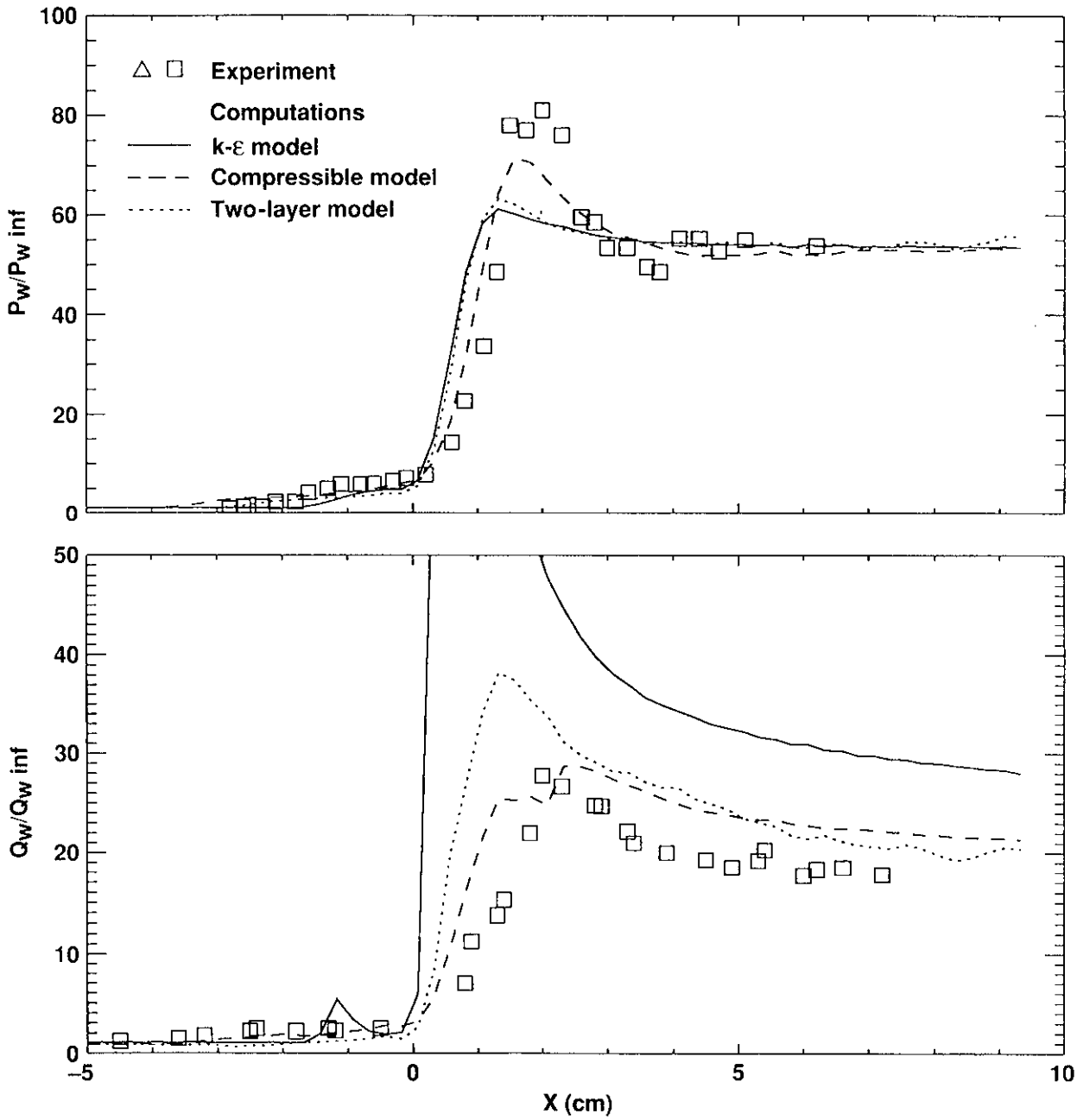

Fig. 11 Comparisons or surface pressure and heat transfer distributions, M = 9.2, 40° cylinder-flare flow.

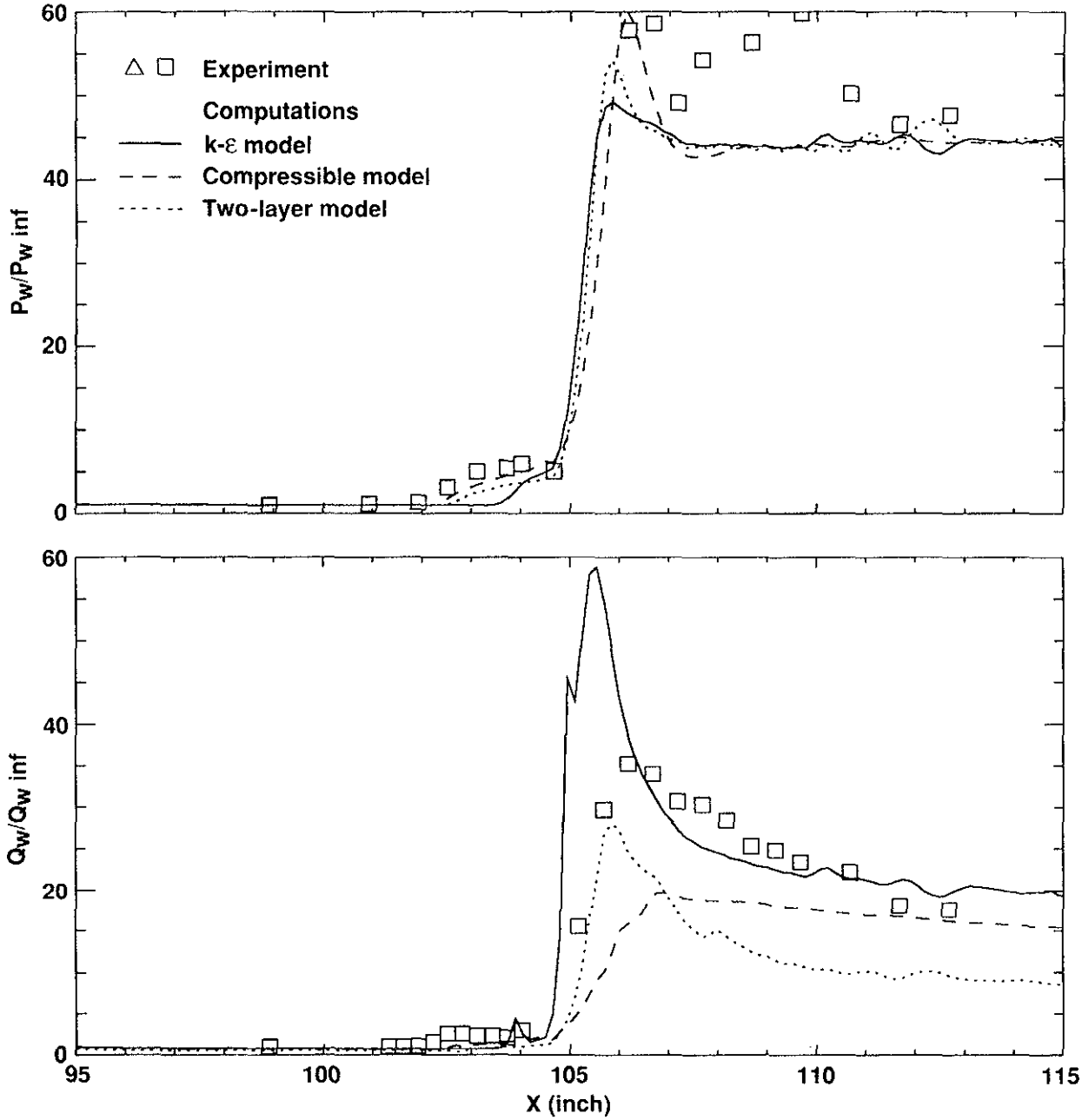

Fig. 12 Comparisons of surface pressure and heat transfer distributions, M = 11, 36° cone-flare flow.

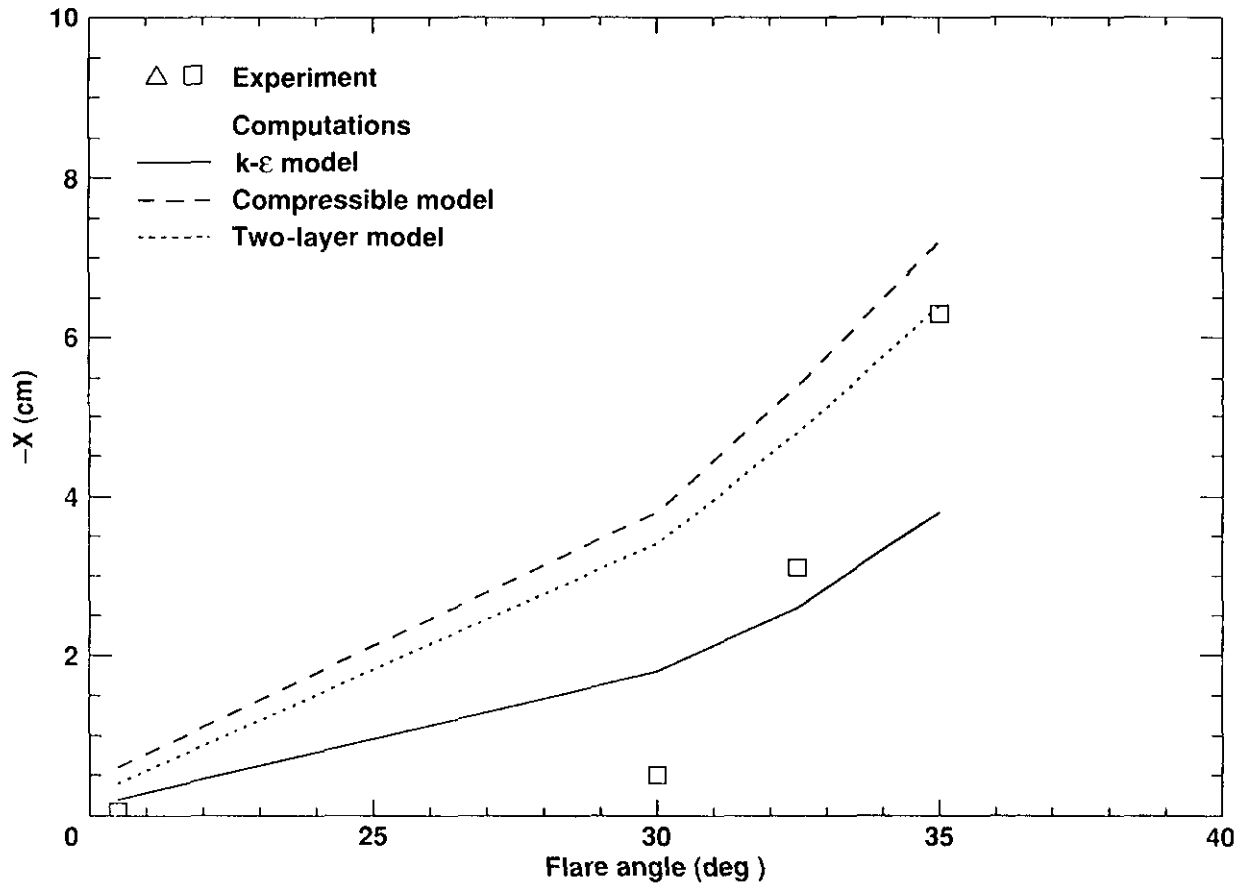

Fig. 13 Comparisons of separation lengths, M = 7.1, cylinder-flare flow.

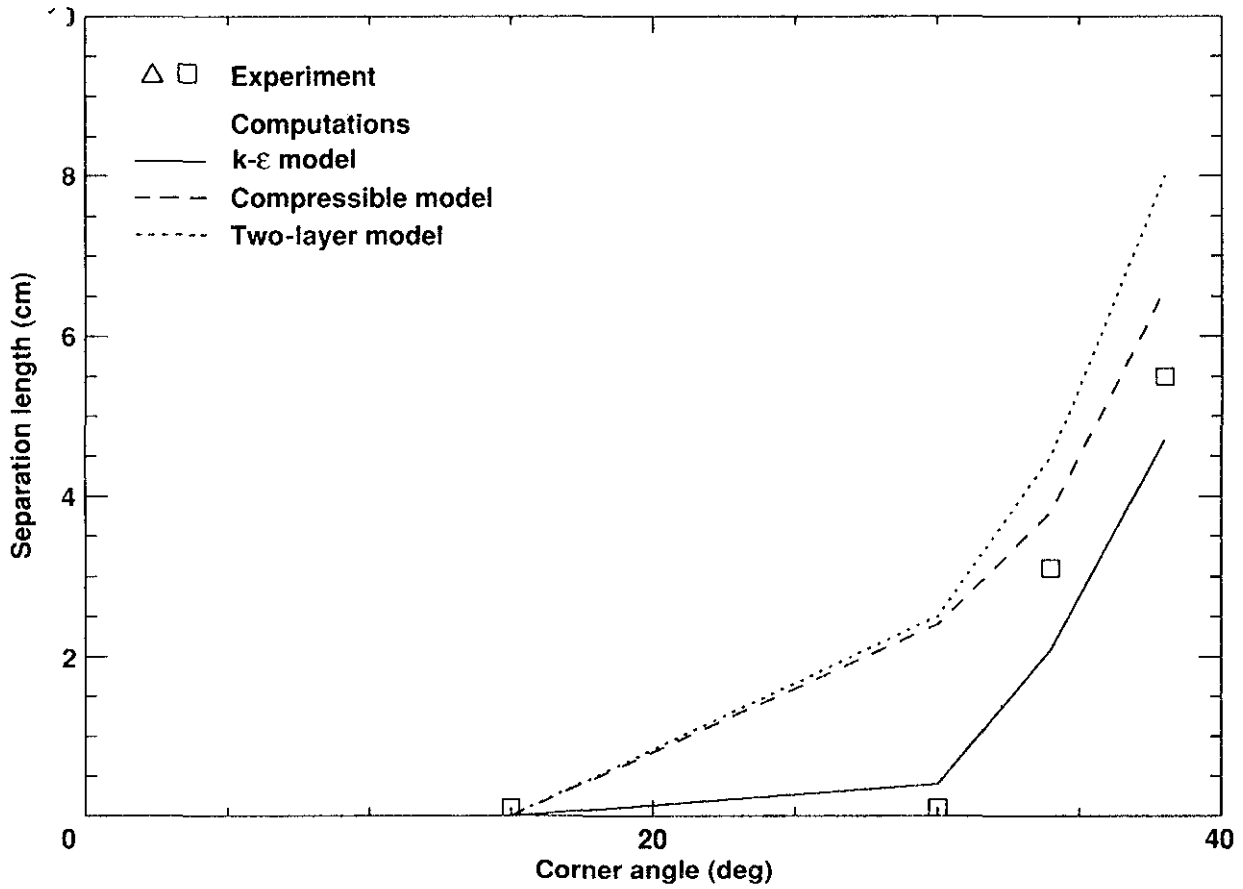

Fig. 14 Comparisons of separation lengths, M = 9.2, compression corner flow.

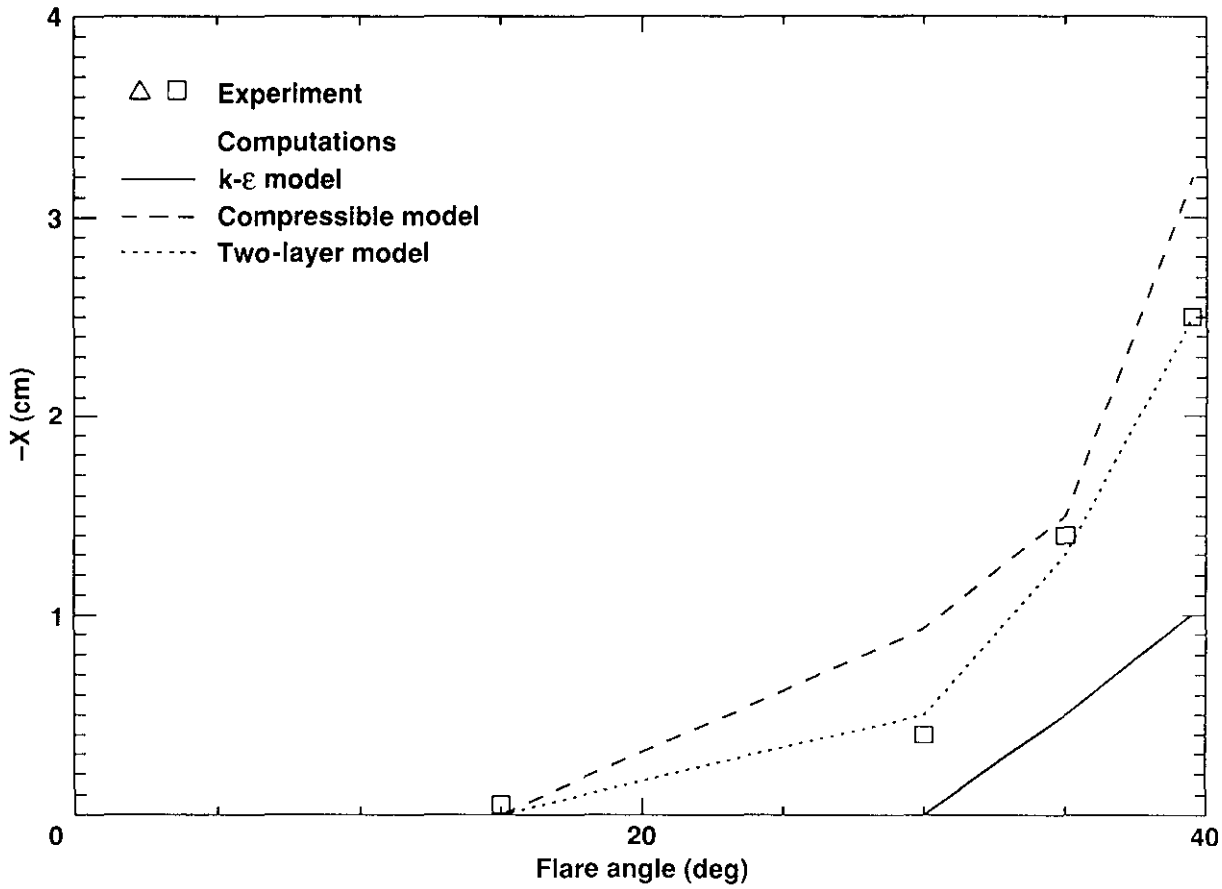

Fig. 15 Comparison of separation lengths, M = 9.2, cylinder-flare flow.

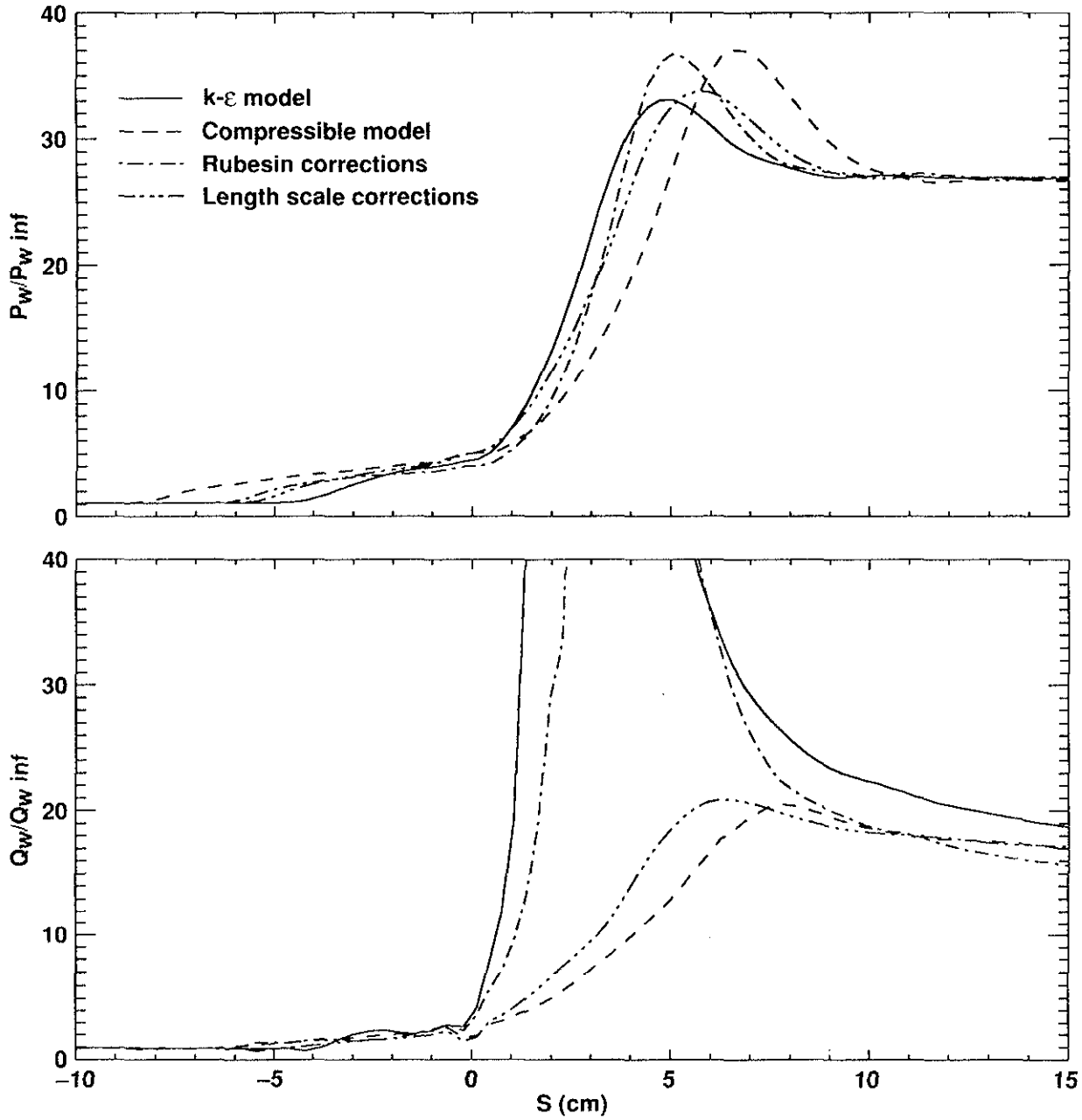

Fig. 16 Effect of individual components of the compressible model, M = 7.1, 35° cylinder-flare flow.

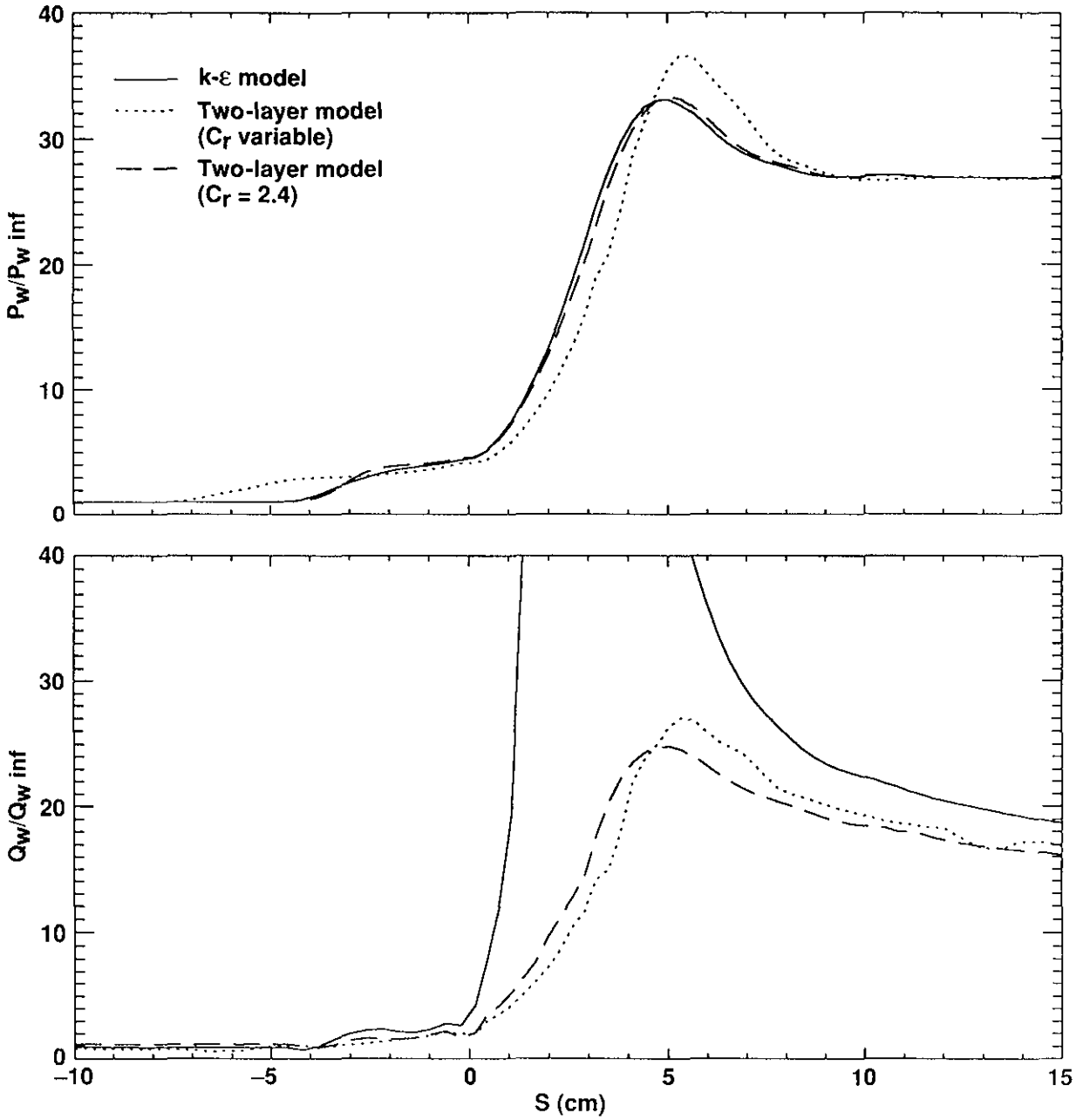

Fig. 17 Effect of constant C_r in the two-layer model, M = 7.1, 35° cylinder-flare flow.